RSC Advances

A green process for efficient lignin (Biomass) degradation and hydrogen production via water splitting using nanostructured C, N, S-doped ZnO under solar light.

Sunil R. Kadam, Vivek R. Mate, Rajendra P. Panmand, Latesh K. Nikam, Milind V. Kulkarni, Ravindra S. Sonawane and Bharat B. Kale*

Simultaneous photocatalytic hydrogen production (water splitting) and waste lignin (Biomass) degradation under visible light has been demonstrated using C, N, S-doped ZnO/ZnS.
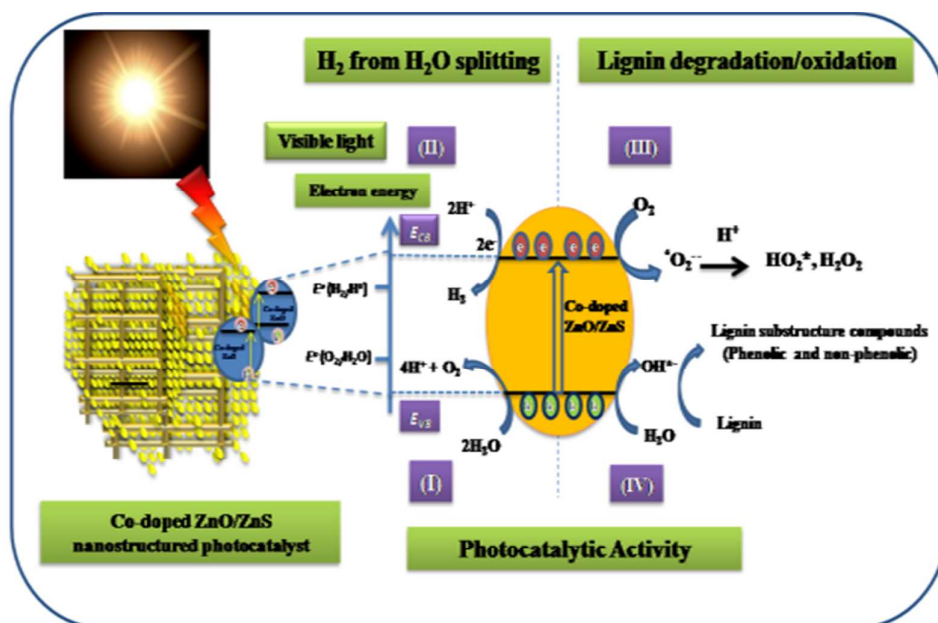
ARTICLE TYPE

Agreen process for efficient lignin (Biomass) degradation and hydrogen production via water splitting using nanostructured C, N, S-doped ZnO under solar light

Sunil R. Kadam, Vivek R. Mate, Rajendra P. Panmand, Latesh K. Nikam, Milind V. Kulkarni, Ravindra
5 **S. Sonawane and Bharat B. Kale***

Herein,we have reported the simultaneous water splitting and lignin (biomass) degradationbyC, N and S-doped ZnO nanostructured material.Synthesis of C, N and S-doped ZnO was achieved viacalcination of
10 Bis-thiourea zinc acetate (BTZA) complex. Calcination of the complex at 500 ^{o}C results in formation of C, N, and S-doping in mixed phase of ZnO/ZnS, while calcination at 600 ^{o}Cgives the single phase of ZnO with N and S doping which is confirmed by XRD, XPS and Raman spectroscopy. The band gap of the calcinedsamples was observed to be in the range of 2.83-3.08 eV.Simultaneous lignin (waste of paper and pulp mills) degradation and hydrogen(H_2) production via water splitting under solar light has been
15 investigated which is hitherto unattempted. The utmost degradation of lignin was observed with the sample calcined at 500 ^{o}C*i.e.* C, N, S-doped ZnO/ZnS as compared to sample calcined at 600 ^{o}C*i.e.* N and S doped ZnO. The degradation of lignin confer the formation of useful fine chemical as a by-product *i.e.* 1-Phenyl-3-buten-1-ol. However, excellent H_2 production *i.e.* 580, 584 and 643 μmole h^{-1} per 0.1g, was obtained for the sample calcined at 500, 550 and 600°C, respectively. The photocatalytic activity obtained
20 is much higher as compared to earlier reported visible light active oxide and sulfidephotocatalysts. The reusability study shows good stability of the photocatalyst. The prima facie observations show that lignin degradation and water splitting is possible with the same multifunctional photocatalystwithout any scarifying agent.

Introduction

25 Recently developing countries are producing more energy at the cost of serious environmental pollutant problems on the planet. It is most important to develop anulternate system which can sustainably minimize environmental problems created by effluents of paper and pulp mills. Effluents from industries such
30 as paper and pulp mills, sugar, etc. cause seriousseveral aquatic and environmental problems. The major contents of effluents are lignin, cellulose, hemicelluloses, molasses, etc.[1,2] Paper and pulp mills alone produce nearly 50 million tonnes of extracted lignin per year as a water soluble by-product (Kraft black liquor) and
35 used as a raw material for synthesis of biofuels and lignin sub-structure.[1,3-5]These have been classified as toxic substances responsible for chemical oxygen demand (COD).[6] In recent years, a promising treatment based on the total oxidation of hazardous organic compounds by using advanced oxidation processes
40 (AOP's) has been reported.[7,8] The common feature of all AOP's is the generation of very reactive free radicals, principally hydroxyl radicals (OH•). The heterogeneous photocatalytic systems (UV active) have been extensively studied due to their ability tophotosensitize the complete mineralization of a wide

45 range of organic substrates (phenols, dyes and pesticides) without the production of harmful by-products.[6,9-13]These catalytic systems having limitations such as photo corrosion of catalyst and requirement of special setup. Moreover, only one target can be achieved either water splitting or degradation of pollutants.
50 Still there is a great potential and necessity forthe development of visible light active photocatalyst.

On the other hand, growing attention about the non-conventional energy for domestic purpose increased due to increased in fuel prices which are born either by depletion of oil
55 resources or its dependency on supply from producer. Amongst the renewable energy resources, solar energy is the largest exploitable resource, and it is estimated that ~0.014% of the solar energy reaching the earth is enough to sustain domestic purpose.[14]The efficient directconversion of solar energy
60 intochemical energy, preferably solar light driven photocatalytic water splitting and degradation of lignin has an immense importance.[15,16] The number of photocatalysts such as TiO_2, TiO_2–graphene, tungsten carbide (WC), zinc oxide (ZnO), zinc sulfide (ZnS), tin oxide SnO_2, *etc*., reported are considered to be
65 the best with respect to H_2 production and lignin degradation in UV light.[6,10,13,17-28] However, widespread use of both TiO_2 and

ultraviolet (UV) light are not economical for large-scale water treatment, thereby interest has been focused towards visible light driven photocatalysis.

To the best of our knowledge there is no report on simultaneous water splitting and degradation of lignin via visible light driven photocatalysis. Therefore, in this manuscript an attempt has been made to examine the both photocatalytic water spitting and degradation of lignin by a multifunctional visible light active photocatalyst. The complete degradation of lignin (sodium salt of lignosulfonate) obtained from industrial site (Vikarabad pulp & paper mills Pvt. Ltd., India) and Aldrich chemical as well as simultaneous H_2 production via water spitting are successfully done by using carbon, nitrogen and sulfur doped ZnO/ZnS (C,N,S-doped ZnO/ZnS) as a solar light active photocatalyst. The research on photocatalytic degradation of lignin using solar light is the effective solution to trim down the pollution caused due to paper & pulp mills. Therefore, the degradation of lignin has also been explored under solar light irradiation. The degradation of lignin conferred the useful fine chemical as a by-product *i.e.*1-Phenyl-3-buten-1-ol. From this, we can achieve maximum clean energy (H_2 production) and at the same time environmental problems caused by lignin contamination in water can be minimised.

Experimental Section

Material preparation

The C,N,S-doped ZnO/ZnS nanostructures was synthesized by the calcination of intermediate prepared from BTZA complex. In a typical synthesis of BTZA, 10 mmol of zinc acetate (99% purity, Qualigens) was dissolved in 50 ml of methanol (95% purity, S.D. Fine Chemicals) under rapid stirring. Simultaneously, thiourea (AR, Qualigens) of 10 mmol was dissolved thoroughly in 50 ml methanol under vigorous stirring. After dissolving both separately, the dissolved thiourea was added drop-wise to the dissolved zinc acetate in methanol solution. This lead to theinstantaneous precipitate formation under stirring. After complete addition of thiourea in zinc acetate solution, white precipitate was formed which indicates the formation of the BTZA complex.[27] This BTZA complex was filtered and washed with methanol and dried at 80 °C for 2 h. Finally, this dried product werecalcined at 500 (S1), 550 (S2), 600 (S3) and 700 °C (S4) for 3 h and are characterized using various technique.

Material characterization

Thermogravimetry (TG) and differential thermal gravimetric analylysis (DTG) of the intermediate was carried out at a heating rate of 10 °C min^{-1} in air (SETARAM-16/18). The crystalline phases and the crystallite size of the photocatalyst was investigated using X-ray powder diffraction (XRD) technique (XRD-D8, Advance, Bruker-AXS).Further, C,N,S-doped ZnO/ZnS samples were examined using X-ray photoelectron spectroscopy (XPS, ESCA-3000, VG Scientific Ltd., England). Room temperature micro Raman scattering (RS) was performed using a HR 800-Raman Spectroscopy, Horiba JobinYvon, France, with an excitation at 632.81 nm by a coherent He–Ne ion laser and a liquid nitrogen cooled CCD detector to collect and process the back scattered data. The optical properties of the powder

samples were studied using an UV-visible-near infrared spectrometer (UV-VIS-NIR, Perkin Elmer Lambda-950). The morphologies of the C,N,S-doped ZnO/ZnS nanostructures were characterized by field emission scanning electron microscopy (FESEM, Hitachi, S-4800) and high resolution transmission electron microscopy (HRTEM, JEOL, 2010F). For HRTEM studies, the samples were prepared by dispersing the powder in ethanol, followed by sonication in an ultrasonic bath for 5 min and then drop-casting the sample on a carbon coated copper grid and by subsequent drying in a vacuum. Specific surface area measurements were done using the BET method (MicromeriticsChemiSorb 2720). The Collected gas sample was analyzedusing a GC system (Shimadzu GC-2025) coupled with TCD detector and packed column (ShinCarbon ST). The liquid sample was analyzed with a gas chromatography with mass spectroscopy (MS) (Shimadzu GCMS-TQ8030) coupled with MS detector and capillary column (FFAP capillary column, 30 m length x 0.32 id). The following temperature program method was used for MS analysis: temperature 45 °C (4 min), 1 °C/min, 60 (o min), 10 °C/min and 250 °C (2 min).

Photocatalytic study

In a typical photocatalytic experiment, 0.02 g lignin (sodium salt of lignosulfonateALDRICH)and 0.1 g of C,N,S-doped ZnO/ZnS photocatalyst (sample S1) was dispersed in 200 ml of deionised water. The whole reaction was carried out in a custom cylindrical quartz photochemical reactor. Before the solution was irradiated, thoroughly purged with argon (Delux, India) to remove all oxygen in the headspace of the reactor and dissolved oxygen in water. A 300 W Xe lamp (LOT ORIEL GRUPPE, EUROPA, LSH302, for Xe lamp spectrum) was used to irradiate the sample with a visible light source, with constant stirring. The amount of hydrogen gas evolved was collected in a graduated glass cylinder (500 ml). All the as prepared (sample S1–S4) and commercial available samples were tested for their catalytic activity under identical conditions. The generated H_2 and O_2gases were collected in a graduated glass cylinder. Finally gases sample were analysed by chromatograph (Shimadzu GC-2025, TCD, argon carrier gas). Apparent quantum yield (QY) was determined with measuring intensity of light with Lux meter (Lutron LX-107HA) and it was placed in front of 300 W Xe light source to obtain the correct wavelength. Apparent quantum yield (AQE) was calculated according to the following equation:

$$AQE\ (\%) = \frac{Number\ of\ H_2\ and\ O_2 molecules\ evolved\ x\ 2}{Number\ of\ incident\ photon} x\ 100$$

Results and Discussion

Fig. 1shows XRD patterns of samples calcined at 200-700 °C. With increasing the temperature from 200 to 400 °C gradual increase in peak intensity at 2θ = 27.5 (100), 48.1 (110) and 56.1 (200) has been observed which is in good agreement with the typical hexagonal phase of the zinc sulfide (JCPDS card no. 01-080-0007). Further, increase in calcinations temperature to 500 °C (S1) shown additional peaks of ZnO along with ZnS peaks at 2θ = 31.8 (100), 34.4 (002), 36.3 (101), 47.5 (102), 56.6 (110), 62.8 (103), 66.4 (200), 68.0 (112) and 69.1 (201) were in good agreement with the reported value for ZnO powder (a = 3.249 Å;

JCPDS card no. 36-1451) and formation of ZnS/ZnO mix phase is confirmed.[19,27] The composition of ZnO:ZnS is found to be 1:1.5 which was calculated from area under deconvoluted peaks of ZnO at 2θ = 31.8 (100), 34.4 (002), 36.3 (101), 68.0 (112) and

5 ZnS peak at 2θ = 27.5 (100) (ESI S-1 Table SI-1 and Figure SI-2). While, we thought that heating of sample at intermediate temperature 550 °C will produce mixed phase composition 1:1, but it shows significantly ZnO phase (JCPDS = 36-1451) (Fig. 1). The XRD of sample calcined at 600 °C (S3) and 700 °C (S4)

10 shows existence of hexagonal wurtzite ZnO structure. While, as-prepared complex shows characteristics peaks of BTZA complex (ESI S-1 Figure SI-1). The crystallite size determined by Scherrerequation was found to be 18, 20, 22 and 32 nm, for S1, S2, S3 and S4 samples respectively.It is quite obvious that the

15 average crystallite size increases with temperature as per crystal growth phenomenon *i.e*. Ostwald ripening.
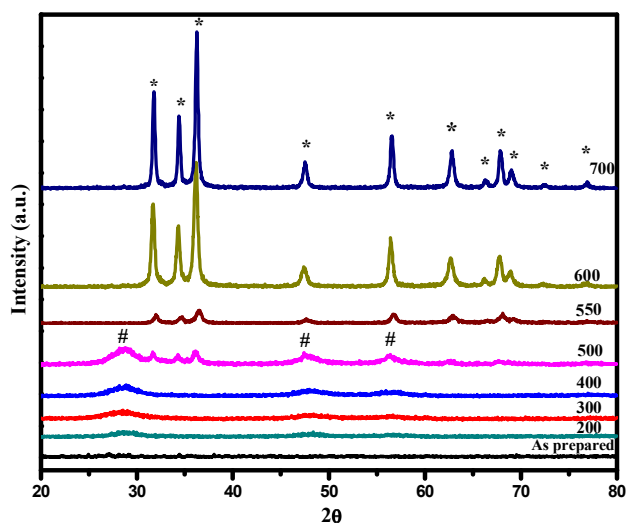
Fig.1XRD pattern of prepared samples. (* zinc oxide peaks and # zinc sulfide peaks).

20 The extent of C, N and S doping into interstitial positions of sampleS1 and S3 were determined by XPS (Fig. 2(A-F)). During the thermal treatment, the complex decomposes into ZnS and ZnO at 500 °C (S1), but sample calcinied at higher temperature 600 °C (S3) shown single phase of ZnO observed in XRD and

25 Raman. The XPS survey spectrum of sample S1 and S3 shows presence of peak assignedto Zn, O, C, N and S elements (Fig. 2(A)). High resolution XPS spectra of the Zn2p and O1s lines are shown in Fig. 2(B). The shifting in core lines at $Zn2p_{3/2}$ and $2p_{1/2}$ is from 1022.1 to 1021.6 eV and from 1045.2 to 1044.8 eV

30 observed in case of sample S1 and S3 respectively. This shifting of $Zn2p_{3/2}$ and $2p_{1/2}$ core lines is by ~0.5 and 0.4 eV, respectively which is due to doping of C, N and Sinto interstitial positions of S1.[29,31]However, due to calcination at higher temperature (600°C) caused the lowering of extent of doping in sample S3 (Fig. 3(B)).

35 [29,31]

The XPS spectrum of O1s is asymmetric in nature which indicates some doping over surface *i.e*. possibility of multi-component oxygen species in the surface region of the samples (Fig. 2(C)). Therefore, spectra was fitted by three Gaussians–

40 Lorentzian located at ~530, 531.5, 531.6 and 533.5 eV (ESI S-2 Figure SI-1). The peak at 531.6 eV corresponds to O_2 adsorbed

on sample surface probably as –OH site.[32] The high energy peaks centred at about 530 and 531.5 eV are (O1s) due to the chemisorbed O_2 atoms coordinated with ZnO/ZnS (S1) and

45 surface –OH, respectively. The peak at 533.5 eV is likely to be due to R-C=S group associated either with Zn or O.[32] It indicates the doping of C, N and S into interstitial positions of the ZnO surface partially via coordinative bond with oxygen. However, intensity of O1s peak slightly increased in case of sample S3 than

50 sample S1 calcined in air (Fig. 2(C)). This clearly indicates the decrease in oxygen deficiency due to calcination, and oxidation of C, N and S. This decrease in doping (N and S) also observed in UV, Raman and XPS (ESI S-2 Table SI-1). The area under the main peaks (530 and 531.5 eV) was found to be higher in S3 than

55 sample S1, which shows decrease in oxygen deficiency (ESI S-2 Table SI-1).

The XPS spectrum for the C1s is shown in the fig. 2(D). Fitting the spectrum with Gaussian–Lorentzian functions, it can be extracted into two components centred at binding energies of

60 279.9 and 284.6 eV in case of sample S1. The component (279.9 eV) can be assigned to the carbon contributions from the R-C=S associated with Zn or trapped interstitial positions in the ZnO/ZnS.[33] The lower binding energy suggests that the carbon may be incorporating into the interstitial positions of the ZnO

65 lattice.[34] These two components (279.9 and 284.6 eV) observed only in case of sample S1 while in case of sample S3 single component (284.6 eV) is observed, which assigned to standard XPS carbon component. This strongly suggests that carbon can be indeed incorporated into the interstitial positions of ZnO/ZnS

70 lattice in case of sample S1, while which is not observed in case of sample S3.

Fig. 2(E) depicts that N1s peaks appeared at 398.4 eV assigned to nitrogen incorporation in ZnO.[29,35] The peaks appeared at 395.0, 396.7, 398.8 and 399.9 eV which indicates nitrogen

75 incorporation which forms N–Zn, N–C, N-C=S and N–H bonds, respectively.[29,36,37] However, with increase in calcination temperature to 600 °C, extent of nitrogen doping lowered in sample S3 than S1 (ESI S-2 Table SI-1). The XPS results are consistent with the interpretation from Raman spectroscopy data,

80 which demonstrate successful N-doping into interstitial positions of both the samples.

The S1s XPS peaks appeared at ~161.3 and 168.6 eV assigned to ZnS and R-C=S, respectively. Indicate formation of ZnS along with C,N,S doped ZnO in sample S1, which is in good agreement

85 with XRD and Raman data (Fig. 3(F)).[38,39] The peak at 161.3 eV (ZnS) disappeared due to calcination at higher temperature (600 °C), while peak at 168.6 eV with lower intensity was observed in case of sample S3, as compared to sample S1. This indicates that in both the samples, sulfur is incorporated into interstitial

90 positions of ZnO.

The percentwise elemental composition of CNS doping present ininterstitial positions ofZnS/ZnO found to be 34:17:49 and 0:28:72 for S1 and S3 samples,respectively (ESI S-2 Table SI-1). This clearly indicates that the percent doping of these C, N and S

95 elements is temperature dependent and one can easily tune this ratio by applying suitable temperature. All above observationsconfirm that sample S1 is of CNS-doped ZnO/ZnS mixed phase material, while sample S3 with nitrogen and sulfur-doping having single phase of ZnO.
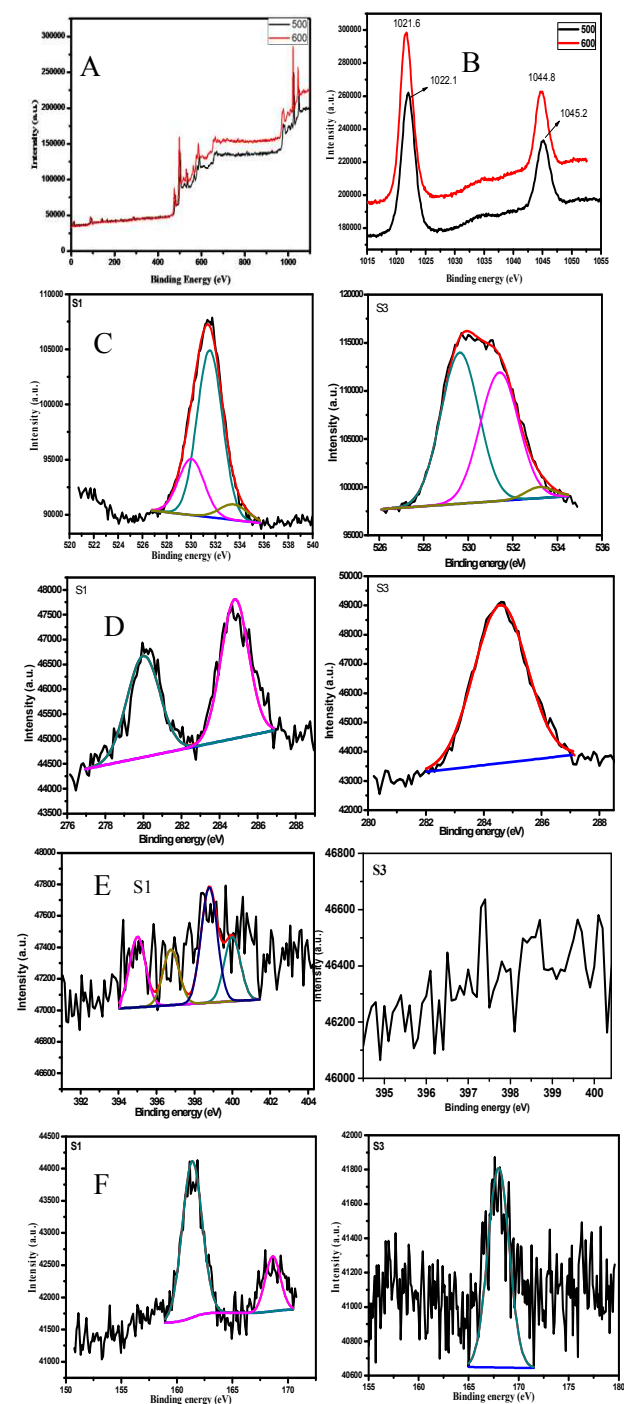
Fig. 2 XPS spectra of S1 and S3 samples (A) XPS survey spectrum, (B) Zinc, (C) Oxygen, (D) Carbon, (E) Nitrogen and (F) Sulfur elements.

Raman scattering was performed for the C,N,S-doped ZnO/ZnS and commercial ZnS samples, as illustrated in Fig. 3. In all the spectra, a common Raman peak is located at 437 cm^{-1} except in commercial ZnS sample (428 cm^{-1}). This peak corresponds to the E2 (high) vibrational mode which implies the existence of the wurtzite structure. The peak located at 333 cm^{-1} corresponds to the second order (E2 (high) − E2 (low)).[40] The other modes are at A1 (278 cm^{-1}), A3 (509 cm^{-1}) and A1 (LO)

(580 cm^{-1}) can be assigned to local vibration modes (LVMs) of nitrogen in ZnO.[41] Raman modes at 278 cm^{-1} was attributed to the localized vibration of Zn atoms, where parts of their first nearest oxygen atoms are partly replaced by nitrogen atom in the ZnO lattice.[42] Also, the Raman peaks observed at 509 and 580 cm^{-1} is related to the presence of nitrogen.[43,44] It is observed that nitrogen related peaks intensity gradually decrease due to calcination at higher temperature (S3 and S4) which is consistent with XPS result. This clearly indicates the nitrogen get escaped at high temperature.

Xue et al. reported S-doped ZnO Raman band located at 1003 cm^{-1} associated with C-S group; however, this is observed at 979 cm^{-1} in our case and it is good agreement with the literature.[45] This might be due to sulfur doping via –C=S group may be effectively shifts Raman band.[46,47] The 1385 cm^{-1} band was attributed to -CO vibration.[40] The 702 and 1100 cm^{-1} bands were attributed to C–S and C-N vibrations respectively, which is matching with the ZnS commercial sample (Fig. 4).[47] When sample heated at higher temperature (600 to 700 °C) gradual decrease in nitrogen related Raman signals intensities were observed as observed in XPS analysis.
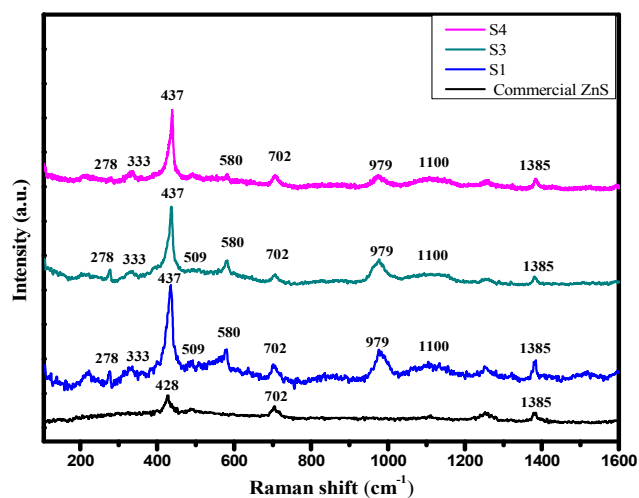
Fig. 3 Raman spectra of commercial ZnS, S1, S3 and S4 samples.

The morphology of the prepared compounds was determined by FESEM (Fig. 4(A-C)). Sample S1 i.e. mixed phase of ZnO/ZnS exhibit three dimensional (3D) nanoplates like structure. These nanoplates are arranged in such a way that it looks like a honeycomb structure. Interestingly, the spherical nanoparticles are located in between the crossed nanoplates. FESEM also shows formation of spherical nanoparticles on the surface of nanoplate. It seems that these nanoparticles originate from the secondary growth of nanoplates due to calcination. The thickness of the nanoplates observed to be 30-50 nm and nanoparticles between the crossed nanoplates are in the range of 30-40 nm. Further, the TEM investigation also shows plate like structure with nanoparticles on the surface. The careful observation convey that there is porous honeycomb like structure which might be due to various possibilities happened during open air calcination such as 1) superficial oxidation of ZnS sheets converted into spherical ZnO nano particles (30-40 nm), 2) due to evolution of gases like

CO_2, NO_2, NH_3, etc. which forms porous morphology and 3) cross linked plate as a result of –C=S, -SO_2, etc., associated with ZnO/ZnS which requires higher temperature to decompose. The formation of ZnO/ZnSmixed phase material is also reveals from
[5] XRD pattern. FESEM of sample S3 shows slightly wavy nanoplates (Fig. 4(B1)). The higher magnified image shows highly crystalline nanoparticles (40-50 nm) on the surface of these wavy nanoplates. Almost similar morphology is observed in case of sample calcined at 700 °C (S4). This change in
[10] honeycomb like porous morphology to spherical nanoparticles might be due to calcination at higher temperature (600 and 700 °C) which might be due to partial or complete oxidation of dopents such as C, N and S.
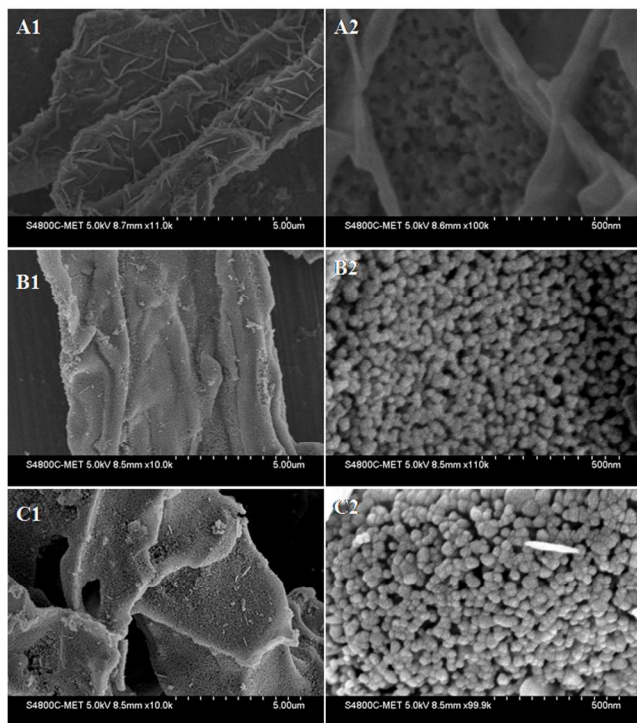
[15] **Fig. 4**FESEM images of (A) S1, (B) S3 and (C) S4 samples.

The crystalline nature and morphology of S1 and S3 was confirmed by using TEM (Fig. 5). Sample S1 were clearly shows the presence of nanoparticles on the surface of nanoplates (Fig. 5(a)). The size of plates and nanoparticles is found to be ~500 and
[20] 30 nm, respectively. At higher magnification, it is seen that the nanoparticles layer is adhered with the nanoplates (Fig. 5(b2)). It suggests that, oxidation start at the surface of sheets of ZnS which is later converted into ZnO. The XRD and Raman study also confirm the formation of mixed phase ZnS and ZnO structure.
[25] Furthermore, the HRTEM image is taken at the surface of ZnO nanoparticles shows interplaner distance ~0.28 nm correspond to (100) plane of wurtziteZnO (Fig. 5(b and b1)). The electron diffraction pattern demonstrates the blur rings due to the polycrystalline nature of sample S1 (ESI S-9 Figure SI-1(a)).
[30] Whereas, TEM image of sample S3 reveals porous sheet like morphology which is composed of ZnO nanoparticles, this might be as a result of complete oxidation of ZnSnanoplates. The size of nanoparticles is observed to be ~ 40-50 nm which is consistent with the FESEM result. The HRTEM image were taken at the

[35] edge of ZnO nanoparticles shows the highly single crystalline nature with lattice fringes 'd' spacing 0.283 nm which correspond to (100) plane of wurtziteZnO (Fig. 5(d)). The formation of ZnO nanoparticles takes place accompanied by a lattice contraction (from 6.188 to 5.206 Å), result in the spherical nanoparticles
[40] morphology.[48-50] When the hexagonal ZnS is completely transformed into WurtziteZnO at calcination temperature of 600 °C, large numbers of nanopores have been formed between the spherical nanoparticles as a consequence of lattice volume contraction during calcination and in this way the matrix released
[45] the tensile stress accumulated in it.[49] It might be due to the doping of S and N which is in consistent with Raman and XPS interpretations. Also, the FFT pattern (Figure 5(d1)) exhibits the hexagonal crystal structure of ZnO. The electron diffraction pattern demonstrates the blur rings pattern due to the different
[50] orientation of nanoparticles (ESI S-9 Figure SI-1(b)).
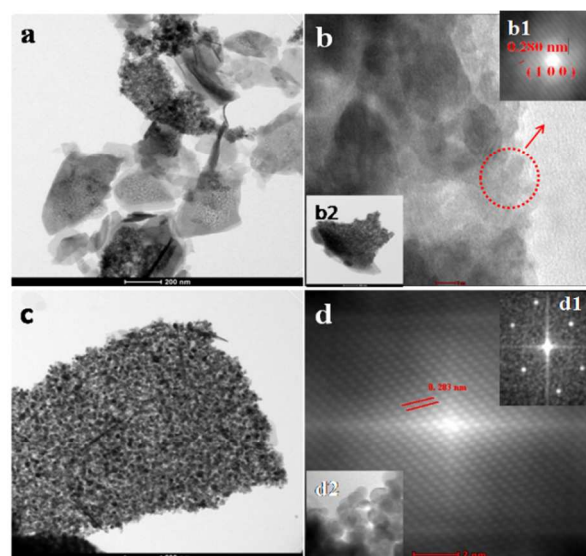
Fig. 5TEM images a, b, b1 and b2 for sample S1 and c, d, d1 and d2 for sample S3 sample.

The UV-visible absorption spectra of doped ZnO sample
[55] annealed at different temperatures presented in Fig. 6(a). The reported absorption cut off edge for commercial ZnO and ZnS samples is ~ 375 and 324 nm, respectively.[19,35] The samples S1 to S4 shows absorption edge cut off at ~438, 427, 403 and 396 nm respectively. The corresponding band gap were found to be 2.8,
[60] 2.9, 3.1 and 3.13 eV of as prepared samples which is slightly blue shifted due to removal of C,N,S doping as shown in S1 to S4, respectively (ESI S-4 Figure SI-1). The energy difference between the aforementioned two features demonstrates the creation of a midgap (deep level acceptor) state in the band gap.
[65] However, in case of sample S4 due to higher calcination temperature (700 °C) there is escape of dopants and hence pure zinc oxide is formed. This suggests that the visible light absorption is due to the introduction of C, N and S into the ZnO/ZnS lattice.
[70] The photoluminescence (PL) measurements is an effective method to investigate the optical characteristics of semiconductor nanomaterials because the information such as surface oxygen defects as well as separation and recombination of photo induced

charge carriers can be obtained. Room temperature PL spectra of as prepared samples were obtained with an excitation wavelength of 350 nm and are shown in Fig. 6(b). The broad green emission band centred at 510 nm is due to the defect created by deficiency
[5] of oxygen observed in sample S1 and S2 , with increase in calcinations temperature (from 500 to 600 °C) the broad emission peak centred at 510 nm is normalized.[51,52]Arbuj et al. reported that the visible emission generally nominated as deep level emission is probably related to the variation of the intrinsic
[10] defects in ZnO, such as vacancy created at surface and interstitial positions due to zinc and oxygen. In a other word, the origin of the visible emission in ZnO is highly controversial.[20,53-56] It is clearly demonstrated that with increase in calcination temperature (from 500 to 700 °C), there is steady decrease in C, N and S
[15] doping due to oxidation of these elements. As a result, oxygen deficiency minimized due to decrease in dopant concentration.
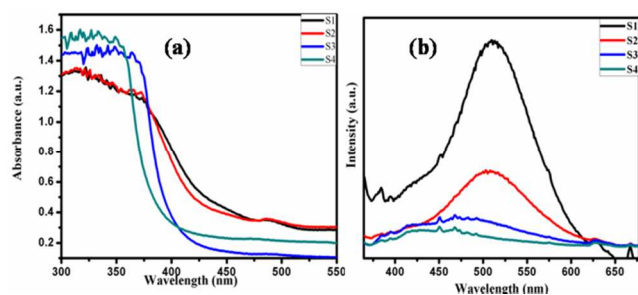
Fig. 6(a) UV-DRS spectra of S1, S2, S3 and S4 samples. (b) PL spectra of S1, S2, S3 and S4 samples.

[20] After careful evaluation of the above all results, the over-all formation mechanism of C, N and S-doping either in mixed ZnO/ZnS or in ZnO phase by the 'thiourea route' can be visualized by Equation 1 and Scheme 1. When zinc acetate and thiourea are mixed in alcoholic medium (methanol) at room
[25] temperature, BTZA complex is formed.[27] We have carried out reaction by keeping zinc acetate to thiourea ratio of 1:2. Further, the complex sample is annealed at 500, 550, 600 and 700 °C on the basis of the precise thermal study by TG-DTA. The thermal study shows multistage weight losses to obtain ZnO/ZnS. Our
[30] foremost endeavour is to dope C, N and S using thiourea, which we have achieved at 500 and 600 °C samples (S1 and S3). On the basis of the critical assignment of weight loss and corresponding endothermic changes in DTA observed during thermal decomposition of the BTZA complex, we have proposed the
[35] reaction mechanism in Scheme 1. According to the TG-DTA (ESI: S-0,Figure S-1), further calcination from 185 °C shows gradual decomposition of the BTZA complex and weight loss in the form of CO_2, NO_2, NH_3, -CH_3, etc. gases as explained in TG-DTA section. The thiourea and its decomposed products such as a
[40] NH_3, NO, -$C=S$, CO, SO, etc., are in intimate contact with the complex and hence the species containing C, N and S in these decomposed products can act as a source for doping in ZnO/ZnS, which is being formed at high temperatures in an air atmosphere.[57] The formation of mixed phase of ZnO_{1-x}(C, N and
[45] S)$_x$ and ZnS in case of 500 °C (S1) is clearly seen in HRTEM. There is a formation of ZnO grain domain on ZnS plate as presented in Scheme1 (S1). These ZnO grain domains are secondary growth of ZnO nanoparticles on ZnS plate. While at 600 °C (S3) single phase of ZnO_{1-x}(NS)$_x$ is already confirmed by

[50] XRD, XPS and Raman. In this case the plate like structure is completely transformed into spherical nanoparticles as presented in Scheme 1. While at 700 °C, pure phase ZnO (S4) has been formed, which is also confirmed by XRD and Raman. This morphological transformation of ZnS to ZnOand C,N,S doping
[55] into it at different temperatures has been presented in Scheme 1.

Eq. (1)

$$xZnO + xZnS + xCS + xNH_2 + xCO_2 + xH_2O + xCO + NO + NO_2$$
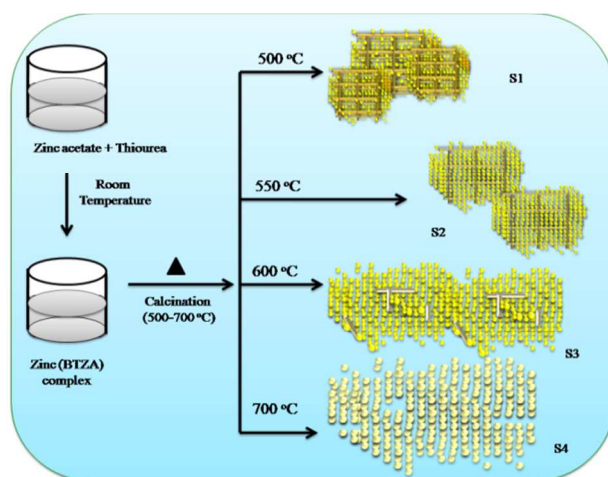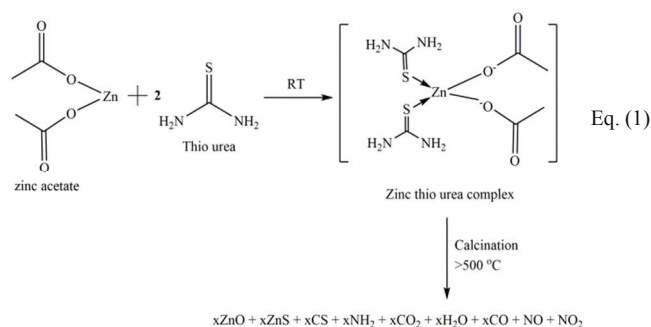
Scheme 1. Schematic representation of formation mechanism of CNS-doped ZnO/ZnS material.

[60] Considering the band gap of doped ZnO in visible region, the photocatalytic activity of lignin degradation and H_2 production by water splitting was performed under visible light. The levels of H_2 production with and without lignin (WWL) over the prepared samples (S1 to S4), and commercial catalysts is shown in Table 1
[65] and Fig. 7. The sample S1 showed 580 and 558 μmol h^{-1}(0.1 g)$^{-1}$(5800 and 5580 μmol h^{-1} g^{-1}) of H_2 generation WWL respectively, which is slightly lower than that of sample S2 (5840 and 5700 μmol h^{-1} g^{-1})and sample S3 (6430 and 6020 μmol h^{-1}g^{-1} WWL) photocatalysts (Table 1 and Fig. 7a and 7b). Surprisingly,
[70] sample S1 shows complete degradation of lignin as well as H_2 production by water splitting under the similar condition (Table 1, ESI S-5 Figure SI-1). This was due to band gap energy 2.83eV, which is ideally in the visible region. Hence, the great amount of electron and holes can be generated by the ZnO/ZnS under visible
[75] light illumination.The H_2 generated by photocatalytic water splitting is analysed by GC (ESI S-6 Figure SI-1). In case of sample S1 the oxygen defects are more therefore, out of total electron generated, some of the electrons are trapped at mid gap state created due to ZnO/ZnS interface. Hence, H_2 production is
[80] slightly lower as compared to that of sample S3. Whereas

photogenerated holes are completely utilized for the lignin degradation in case of sample S1 which is not observed in sample S3. While, sample S4 showed two times (276 and 223 μmol h^{-1} (0.1 g)$^{-1}$ WWL) lower H$_2$ production than sample S1, S2 and S3 respectively (Table 1). Thus, decrease in activity of sample S4 is quite understood due to higher band gap *i.e.* 3.13 eV which is in UV region.Since, there is no much difference in particles size, it is not wise to account for enhancement,though it will contribute some extend in all samples.

Table 1 Photocatalytic activity for lignin (Biomass) degradation and water splitting using nanostructured CNS-doped ZnO/ZnS visible photocatalyst

Catalysts	Surface area (m^2/g)	Average H$_2$ generation (μmol h^{-1})		Apparent quantum yield	
		With Lignin	Without Lignin	With Lignin	Without Lignin
S1	74.7	580^	558	14.16^	13.33
S2	51.1	584	570	14.51	13.91
S3	39.4	643	602	15.05	14.25
S4	33.8	276	223	8.10	5.10
Commercial ZnO	-	89	22	2.09	0.53
Commercial ZnS	-	156	45	3.76	1.07
¥	-	205	45	5.00	1.02
Blank run	-	89	<0.1	2.08	<0.1
S1#	74.7	535	527	13.47	12.4
S1*	74.7	584	553	14.26	13.50

Reaction conditions : catalyst, 0.1 g; water, 200 ml; Lignin, 100 ppm, Xe lamp, 300 W (Oriel).

^ Standrad deviation is 0.957 and 0.019, in case of Volume of H$_2$ generation and apperant quantum yield, respectively.

¥ Physical mixture of commercial ZnO and ZnS catalysts.

# Indicates the activityof catalyst after fourth recycle.

* Indicates the industrial (Vikarabad Pulp & Paper Mills Pvt. Ltd., India) sample of lignin.

The repeatability of the H$_2$ production with lignin for catalyst S1 was observed with good precision (standard deviation 0.957 and 0.019 in case of volume of H$_2$ generation and quantum yield ,respectively).The sample S1 found to be retaining its activity after fourth recycle,which prove the stability of catalyst (Table 1, ESI S-4 Figure SI-2). Interestingly, lignin sample collected from industrial site (Vikarabad pulp & paper mills Pvt. Ltd., India) showed equivalent activity in terms of both water splitting and degradation of lignin. This indicates the suitability of sample S1 for industrial lignin sample and one can think effective utilization of sustainable resources for cleaner energy and water purification simultaneously where both are available abundantly. Furthermore, MS of intermediate step sample shows presence of 1-Phenyl-3-buten-1-olwhich is having resemblance with lignin sub-structured compound (ESI S-6 Figure SI-2). Further, study with details investigation is in progress. It is quite interesting and curious that sample S1 confer H$_2$ production as well as lignin degradation (ESI S-6 Figure SI-1 and SI-2). Sample S3 shows highest H$_2$ production with lignin and slightly less without lignin. However, we could not observe lignin degradation using sample S3. It seems presence of lignin decreases electron (e$^-$) and hole

(h$^+$) recombination. If we consider the photoluminescence, there is drastic decrease in the intensity of emission peak in case of samples S2 and S3 indicating that excitonic electron in the conduction level of the semiconductor are transferred to the surface which is utilize for H$_2$ evolution reaction.[16,56] However, further study is in progress to know the role of lignin in photocatalysis reaction. It is to be noted that the all reaction have been performed without sacrifying agent.This is quite intresting and also call the very serious discussions.There might be utilization of holes for lignin degradation and electrons for water splitting. Hence, lignin may playing role of scarifying agent. However, it needs to examine thoroughly which is in progress.Rao et al. clearly mentioned that there is a formation of H$_2$O$_2$with in the reaction in absence of scarifying agent.[58] Hence, we feel that the same phenomenon might have taking place in present case. In presence of lignin, slight increase in H$_2$ may be due to the lignin which may be acting as a scarifying agent

Then possibility is either mixed phase composition or co-doping are responsible for this remarkable activity. Hence, we have performed photocatalysis using individual and physical mixture of commercial ZnO and ZnSphotocatalysts (Table 1 and ESIS-5 Figure SI-1)**.** The individual ZnO and ZnS samples showed lower activity WWL as compared to sample S1, respectively (Table 1). However, in physical mixture ZnO: ZnS with 1:1.5 composition showed higher activity than the individual samples and lower than sample S1 (Table 1). This clearly indicates that mixed phase plays key role in enhancement of photocatalytic activity.

Fig. 7c presents UV-visible absorption spectra of the (%) lignin degradation with respect to time by using sample S1. It reveal that with increase in time gradual decrease of lignin peak intensity was observed. The complete degradation of 100 ppm lignin is achieved within 5 hours in presence of 100 mg S1 photocatalyst (Fig. 7(c)). However, 1000 mg S1 photocatalyst show complete degradation of lignin within 1 hour. We also observed with increase in catalyst, lignin degradation rate is increased but hydrogen production is constant after 200 mg catalyst loading. Significantly, this might be due to effectively decrease in electron at conduction level where as availability of holes preferentially facilitates degradation of lignin rather than water splitting (ESI S-5 Table SI-1).

In the literature, it is well reported that heterogeneous photocatalytic degradation reactions follows pseudo first order kinetics.[56,59]The first order reactions follows the rate law which indicates rate of degradation depends on concentration of reactants (2)

$$Rate = -\frac{dc}{dt} = K_{obs}C \qquad (2)$$

Where K$_{obs}$is the observed rate constant of the degradadtion reaction and C is the concentration[60].

The reaction kinetics for heterogeneous photocatalytic degradation of lignin has been studied and plot of (%) lignin degradation versus time (h) andln (C$_0$/C$_t$) versus time (h) wereplotted and shown in ESI S-7 Figure SI-1(a) and (b) respectively. The slope of this plot gives rate constant values as per reaction kinetics of first order reaction.The rate constant for photocatalyticlignin degradation using 100 mg S1 photocatalyst found to be 0.1005 h^{-1}. Among the prepared catalyst, sample S1 is

the best photocatalyst due to its excellent activity and stability in both H_2 production (water splitting) as well as complete degradation of lignin. However, sample S3 showed slightly higher H_2 production but did not shown lignin degradation. Photocatalytic activity obtained for all synthesized samples (S1-S4) is higher than the commercial ZnO, ZnS and its physical mixture samples. In a nutshell, sample S1 was observed to be versatile photocatalyst which shows good photocatalyticH_2 production performance and complete lignin degradation.
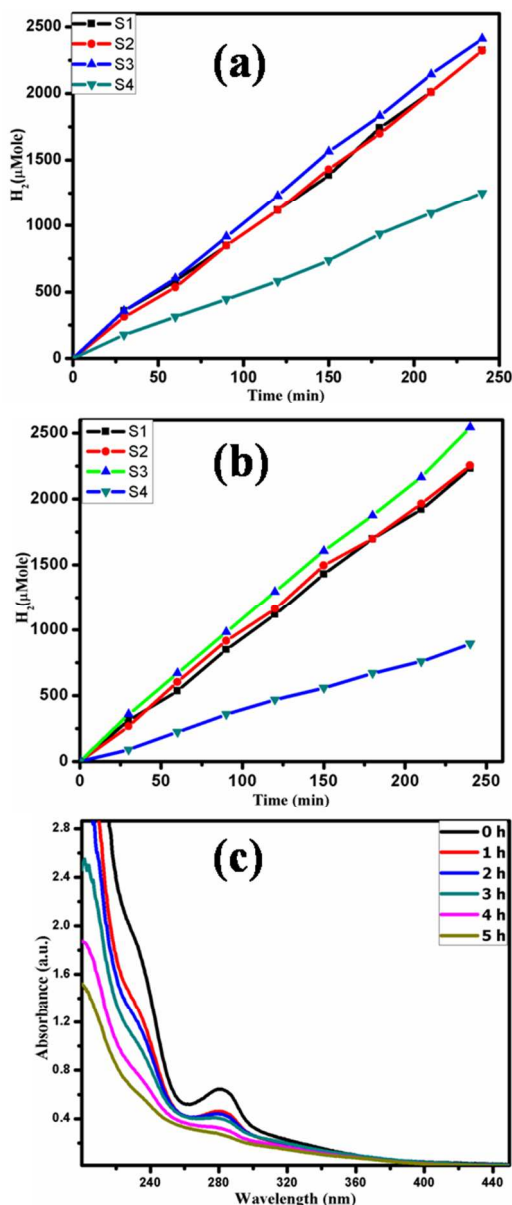
Fig. 7(a) Photocatalytic water splitting in presence of lignin using S1, S2, S3 and S4 samples (b) Photocatalytic water splitting without lignin using S1, S2, S3 and S4 samples (c) Photocatalytic degradation of Lignin (100 ppm) by using S1 catalyst. (Reaction conditions: catalyst, 0.1 g; water, 200 ml; Lignin, 100 ppm Xe lamp, 300 W (Oriel)).

Conclusions

In conclusion, the C, N and Sdoped mixed phase ZnO/ZnS nanostructure (sample S1) has been synthesized by thermal decomposition of BTZA complex at 500°C. Further calcinations at 600 °C (S3) confer the N and S doped ZnO which is ensuredfrom XRD, Raman and XPS studies. Surprisingly, sample S1 shows superior activity for both H_2 production (580 and 558 µmole h^{-1} per 0.1 g WWL) via water splitting as well as complete degradation of lignin under visible light, simultaneously. This is due to its novel characteristics such as lower bandgap 2.83 eV. The C,N,S-doping in ZnO/ZnSnanostructure and unique honeycomb like structure. Whereas, the sample S3 shows very less degradation of lignin but, it shows higher activity for H_2 production (643 and 602 µmole h^{-1} per 0.1 g WWL). The water splitting results also showed increasedhydrogen generation with increase in catalyst up to an optimum loading (from 100 to 200 mg), while further increase in catalyst (from 200 to 1000 mg) does not show any enhancement in H_2 production. Interestingly, the lignin degradation increased linearly with increase in catalyst dose. Most importantly, lignin degradation proceeds via degradation of basic unit (phenols and polyphenols)which is identified by analyzing reaction intermediate via MS. From MS analysis it is observed, there is formation of different product such as 1-Phenyl-3-buten-1-ol, 3-Hydroxy-2-methyl-3-phenyl-propionic acid and Methyl hydroxyl (phenyl) acetate.However, the major content of produced during photocatalysisis finechemicals (1-Phenyl-3-buten-1-ol) from polymeric lignin via use of sustainable resources. The process is clearly basic and applicable to most of the paper and pulp mills. We have also discussed sustainable reuse of polluted sample released from paper and pulp mills for the production of clean fuel (H_2) and effectively clean water using C, N and Sdoped ZnO/ZnS nanostructure catalyst under visible light. It is noteworthy that all photocatalytic reactions are performed without any scarifying agent.

Acknowledgements

Notes and references

Centre for Materials for Electronics Technology,
Department of Electronics and Telecommunication (DeitY),
Govt. of India, Panchawati, Off Pashan Road,
Pune-411008, India. bbkale@cmet.gov.in

1   J. Zakzeski, P. C. A. Bruijnincx, A. L. Jongerius and B. M. Weckhuysen, *Chem. Rev.* 2010, **110**,3552-3599.
2   M. Saidi, F. Samimi, D. Karimipourfard, T. Nimmanwudipong, B. C. Gates and M. R. Rahimpour, *Energy Environ. Sci.*2014, **7**, 103-129.

3   V. R. Mate, M. Shirai and C. V. Rode, *Catal. Commun.*2013, **13**, 66-69.

4   R. Ma, M. Guo and X. Zhang, *ChemSusChem.* 2014,**7**, 412-415.

5   S. Nanayakkara, A. F. Patti and K. Saito,*Green Chem.* 2014, DOI: 10.1039/c3gc41708e.

6   M. A. Fox and M. T. Dulay, *Chem. Rev.* 1993, **93**, 341-357.

7   P. Peralta-Zamora, S. G. de Moraes, R. Pelegrini Jr., M. Freire, H. D. Mansilla and N. Duran, *Chemosphere*1998, **36**,2119-2133.

8   K. H. Wang, Y. H. Hsieh, M. Y. Chou and C. Y. Chang, *Appl. Catal. B-Environ.*1999, **21**,1-8.

9   N. Serpone and E. Pelizzetti in *Photocatalysis: Fundamental and applications* Wiley/Interscience, 1989.

10   A. A. Khodja, T. Sehili, J. F. Pilichowski and P. Boule, *J. Photoch. Photobio. A*2001, **141**, 231-236.

11   S. K. Kansal, M. Singh and D. Sud, *J. Hazard. Mater.* 2008, **141**, 581-590.

12   S. Lathasree, R. Nageswara, B. Sivasankar, V. Sadasivam and K. Rengaraj, *J. Mol. Catal A-Chem.*2004, **223**,101-105.

13   E. Kusvuran, A. Samil, O. M. Atanur and O. Erbatur, *Appl. Catal. B-Environ.*2005, **58**, 211-216.

14   N. Lewis and D. G. Nocera, *P. Natl. Acad. Sci. U. S. A.* 2006, **103***, 15729-15735.

15   W. Fan, Q. Zhang and Y. Wang, *Phys. Chem. Chem. Phys.*2013, **15**, 2632.

16   http://www.iea.org/topics/solarpvandcsp.

17   A. Kudo, *Int. J. Hydrogen Energ.*2007, **32**,2673-2678.

18   S. Gawande and S. R. Thakare, *ChemCatChem*2012, **4**, 1759-1763.

19   S. K. Apte, S. N. Garaje, S. S. Arbuj, B. B. Kale, J. O. Baeg, U. P. Mulik, S. D. Naik, D. P. Amalnerkar and S. W. Gosavi, *J. Mater. Chem.*2011, **21**,19241-19248.

20   S. S. Arbuj, N. Rumale, A. Pokle, J. D. Ambekar, S. B. Rane, U. P. Mulik and D. P. Amalnerkar, *Sci. Adv. Mat.*2014, **6**,1-7.

21   K. Kobayakawa, Y. Sato, S. Nakamura and A. Fujishima, *Bulletin of Chemical Society of Japan*1989, **62**, 3433-3436.

22   K. Tanaka, R. C. R. Calanag and T. Hisanaga, *J. Mol. Catal. A-Chem.*1999, **138**,287-294.

23   M. Ksibi, S. B. Amor, S. Cherif, E. Elaloui, A. Houas and M. Elaloui, *J. Photoch. Photobio. A* 2003, **154**,211-218.

24   L. Liu, Z. Liu, A. Liu, X. Gu, C. Ge, F. Gao and L. Dong, *ChemSusChem*, 2014, **7**, 618-626.

25   A. T. Garcia-Esparza, D. Cha, Y. Ou, J. Kubota, K. Domen and K. Takanabe, *ChemSusChem*, 2013, **6**, 168-181.

26   Y. S. Ma, C. N. Chang, Y. P. Chiang, H. F. Sung and A. C. Chao,*Chemosphere*2008, **71**, 998–1004.

27   R. Prado, X. Erdocia and J. Labidi,*Chemosphere*2013, **91**, 355–1361

28   L. C. Chen, Y. J. Tu, Y. S. Wang, R. S. Kan and C. M. Huang,*Journal of Photochemistry and Photobiology A: Chemistry*2008, **199**, 170–178.

29   A. P. Bhirud, S. D. Sathaye, R. P. Waichal, L. K. Nikam and B. B. Kale, *Green Chem.*2012, **14**,2790-2798.

30   J. J. P. Thomas and L. R. Ruby, *Int. J. Comput. Appl.*2010, **6**,7-11.

31   D. Briggs and M. P. Seah, WILLEY & SONS. Vol. **1**, Second Edition, 1993.

32   S. F. Chen, S. J. Zhang, W. Liu and W. Zhao, *J. Hazard. Mater.*2008, **155**, 320-326.

33   X. B. Liu, H. J. Du, X. W. Sun, B. Liu, D. W. Zhao and H. D. Sun, *CrystEngiComm.*2012, **14**,2886-2890.

34   J. L. Zhai, L. L. Wang, D. J. Wang, Y. H. Lin, D. Q. He and T. F. Xie, *Sensors Actuat. B-Chem*. 2012, **161**, 292-297.

35   M. Mapa and C. S. Gopinath, *Chem. Mater.*2009, **21**, 351-359.

36   H. Wang, H. P. Ho, K. C. Lo and K. W. Cheah, *J. Phys. D Appl. Phys.*2007, **40**, 4682-4685.

37   C. L. Perkins, S. H. Lee, X. Li, S. E. Asher and T. J. Coutts, *J. Appl. Phys.*2005, **97**, 034907.

38   A. Galtayries and J. Grimblot, *J. Electron Spectrosc.*1998, **98-99**,267-275.

39   J. Wang, J. F. Lu, Q. W. Zhang, S. Yin, T. Sato and F. Saito, *Chemistry for sustainable development*, 2007, **15**, 249-253.

40   J. Serrano, A. H. Romero, F. J. Manjon, R. Lauck, M. Cardona and A. Rubio, *Phys. Rev. B*2004,**69**, 094306.

41   K. Saito, Y. Hosokai, K. Nagayama, K. Ishida, K. Takahashi, M. Konagai and B. P. Zhang, *Journal of Cryst. Growth* 2004, **272**,805-809.

42   X. Zhu, H. Z. Wu, D. J. Qiu, Z. Yuan, G. Jin, J. Kong and W. Shen, *Opt. Commun.*2010,**283**, 2695-2699.

43   B. Sieber, H. Liu, G. Piret, J. Laureyns, P. Roussel, B. Gelloz, S. Szunerits and R. Boukherroub, *J. Phys. Chem. C*2009,**113**, 13643-13650.

44   G. T. Du, Y. Ma, Y. T. Zhang and T. P. Yang, *Appl. Phys. Lett.*2005,**87**, 213103.

45   F. Xue and J. Liang, *Spectrochim. Acta A*2011,**83**, 348-352.

46   G. T. Meng, J. C. K. Chan, D. Rousseau and E. C. Y. Li-Chan, *J. Agr. Food Chem.*2005, **53**, 845–852.

47   A. Synytsya, P. Alexa, J. de Boer, M. Loewe, M. Moosburger, M. Wurkner and K. Volka, *J. Raman Spectrosc.*2007, **38**, 1646-1655.

48   J. S. Jang, C. J. Yu, S. H. Choi, S. M. Ji, E. S. Kim and J. S. Lee, *J. Catal.*2008, **254**,144-155.

49   J. S. Jang, E. S. Kim, S. H. Choi, D. H. Kim, H. G. Kim and J. S. Lee, *Appl. Catal. A*2012,**106**, 427-428.

50   H. Fu and J. Li, *J. Chem. Phys.*2004, **120**, 6721-6727.

51   Y. Zheng, J. Zhu, C. Chen, Y. Zhu, Y. Zhan, X. Lin, Q. Zheng and K. Wei, *Inorg. Chem.*2007, **46**, 6675-6682.

52   Xiu-hua Wang and S. Liu, *Chinese J. Chem. Phys.*2007, **20**, 632-636.

53   Y. Yang, H. Yan, Z. Fu, B. Yang, L. Xia, Y. Xu, J. Zuo and F. Li, *Solid State Commun.*2006,**138**, 521-525.

54   K. Vanheusden, C. H. Seager, W. L. Warren, D. R. Tallant and J. A. Voigt, *J. Appl. Phys.*1996, **79**, 7983-7990.

55   V. G. Pol, J. M. Calderon-Moreno and P. Thiyagarajan, *Langmuir*2008, **24**, 13640-13645.

56   M. Trejo, P. Santiago, H. Sobral, L. Rendon and U. Pal, *Cryst. Growth Des.*2009, **9**, 3024-3030.

57   C. Giordano, C. Erpen, W. Yao, B. Milke and M. Antonietti, *Chem. Mater.*2009, **21**, 5136-5144.

58   M. V. Rao, K. Rajeshwar , V. R. Pai Verneker , J. DuBow, *J. Phys. Chem.*, 1980, **84 (15)**, 1987–1991

59   S. Chakrabarti and B. K. Dutta, *J. Hazard. Mater.* 2004, **112**, 269-278.

60   S. Khezrianjoo, H. D. Revanasiddappa, *Chemical Sciences Journal*, 2012, 2012 **(CSJ-85),** 1-8.